

Chemical Evolution in Galactic Nuclear Discs

Jennifer K. S. Friske,^{1*} Ralph Schönrich,¹

¹*Mullard Space Science Laboratory, University College London, Holmbury St. Mary, Dorking, Surrey, RH5 6NT, UK*

Accepted XXX. Received YYY; in original form ZZZ

ABSTRACT

Nuclear Stellar Discs have been observed in the vast majority of barred disc galaxies including the Milky Way. Their intense star formation is sustained by the intense gas inflows driven by their surrounding bars and frequently supports a large-scale galactic fountain. Despite their central role in galaxy evolution, their chemical evolution remains largely unexplored. Here we present the first systematic, multizonal modelling of the chemical evolution of these nuclear stellar discs. We argue that the chemical composition of nuclear stellar discs is best understood relative to the bar tips from which their gas is drawn. We make predictions of the detailed abundance profiles within the nuclear stellar disc under different accretion scenarios from the galactic bar and show by which observable differences they can be decided. We show that with their difference to normal disc star formation, nuclear discs offer a unique laboratory to break parameter degeneracies in chemical evolution models. This allows us to identify the effects of the main gas parameters and disentangle them from the global enrichment history. We show this for the example of the ejection fractions from the outer and nuclear disk.

Key words: galaxies: abundances, evolution, structure – Galaxy: abundances, evolution, centre

1 INTRODUCTION

This paper aims to connect chemical evolution modelling to the physics and history of Galactic nuclear stellar discs (NSDs). The paper has two aims: establish a chemical evolution framework that links NSD abundances to their structure, and second, to target parameter degeneracies in chemical evolution models by using NSDs as unique laboratories.

Galactic NSDs are commonly found in the centres of barred galaxies including our own Milky Way, where the central stellar density cusp (e.g. [Launhardt et al. 2002](#); [Chatzopoulos et al. 2015](#)) was recently proven to be a rotating NSD ([Schönrich et al. 2015](#)) with comparably cold kinematics that contrast strongly with the surrounding bulge. The principles of NSD formation are qualitatively well understood, as galactic bars funnel large amounts of gas into the central region of galaxies where it is largely deposited onto intensely star-forming rings on the edge of NSDs. We will describe this in more detail in [section 2](#).

While the general principles in the nuclear stellar disc formation are clear, little to nothing is known about their structure and evolution: we can find no reliable information how the material funneled onto the nuclear discs is redistributed beyond the star-forming ring, i.e. if the funneled gas flows radially inwards through the NSD, or is otherwise also directly deposited further in. We lack information on the loss of gas and stellar yields from NSDs, the mode of their apparent growth in size, other accretion mechanisms, internal migration/redistribution of stars, impact by the nearby AGNs, etc.

Here a chemical evolution framework can provide answers: since their inception ([Burbidge et al. 1957](#); [Alpher et al. 1948](#); [Arnett & Clayton 1970](#); [Pagel & Patchett 1975](#)), chemical evolution models

have been used to show that galaxies must follow an open rather than closed box scheme with consistent inflow of fresh material ([Tinsley 1979](#)), the radial abundance gradients have been quantitatively connected to inside-out formation ([Schönrich & McMillan 2017](#)) and the mode of gas accretion from the corona ([Bilitewski & Schönrich 2012](#)), and e.g. stellar metallicities have been used, in conjunction with chemical evolution models, to measure radial migration of stars. Other detailed models have been used to constrain cosmic infall ([Colavitti et al. 2008](#), see e.g.), stochastic chemical evolution in the halo (e.g. [Matteucci & Chiosi 1983](#); [Karlsson 2005](#); [Cescutti 2008](#)), or to play on the stellar initial mass function (IMF).

To achieve this, a full multi-zone chemical evolution model of the galactic centre must be drawn up and compared to the data. However, apart from a pioneering one-zone model by [Grieco et al. \(2015\)](#) (also used in [Thorsbro et al. 2020](#)) which covered some of the important aspects, no such work appears to have been undertaken. We will also make the point that our models are largely of predictive nature at current stage, because no sufficient data have been gathered on NSD abundances. Such comparisons have rather simple structure with powerful implications. E.g. the overall metal content of NSDs can directly quantify the loss of yields and gas from the nuclear disc, by this quantifying (together with the total stellar mass) the total amount of gas that has been funnelled by the bar, and by this the angular momentum transfer to the bar. This angular momentum transfer has various important consequences and is e.g. essential to quantifying the angular momentum loss of the (slowing) bar to the dark halo and by this quantifying the structure of the dark halo ([Chiba et al. 2020](#); [Chiba & Schönrich 2021](#)).

Further than the study of nuclear disc physics, chemical evolution models are in dire need of different laboratories than galactic discs to break weakly constrained parameter degeneracies in chemical evolution. As one important example, it has been noted that the only way

* E-mail: jennifer.friske.20@ucl.ac.uk

to resolve the chemical evolution of r-process elements with significantly super-solar $[r - \text{process}/\alpha]$ ratios (Côté et al. 2018, 2019) is using a two phase interstellar medium (ISM) and having a higher contribution fraction of neutron star mergers to the cold gas phase than core collapse supernovae (by a factor ~ 2 , see Schönrich & Weinberg 2019; Fraser & Schönrich 2021). However, this hot/cold gas phase separation introduces a whole set of new parameters, that thus far are only constrained by this single observation, as chemical evolution becomes insensitive to this parameter at timescales larger than the hot gas cooling timescale (~ 1 Gyr). We show here that given the large expected loss rates of hot gas, the nuclear stellar disc can display a permanent different in abundance ratios, thus breaking this parameter degeneracy.

The paper is structured as follows: We will first give an overview of the necessary theoretical background about chemical evolution and the current state of the research about nuclear stellar discs in section 2. Then, we introduce the models used and the adjustments made to accommodate a nuclear disc in section 3, before exploring two main accretion and inflow histories. Discussing the general effect a nuclear disc has on the global chemical evolution then sets the stage to pin down the effects different global and local gas parameters as well as inflow histories have on the gas composition in section 4, before giving a quick outlook on future work in section 5.

2 BACKGROUND

2.1 Elemental Abundances

Chemical evolution models connect physical parameters of a system to the chemical composition of ISM and stars vs. age and position. The star formation history, accretion, etc. in a galaxy affect the enrichment of the star-forming ISM with processed gas from previous generations as shown in Figure 1. However, age measurement uncertainties hamper using the age-dependence, so already Tinsley (1979) studied instead abundance planes using abundance ratios as chemical clocks:

$$[X/\text{Fe}] = \log_{10} \frac{n_X}{n_{\text{Fe}}} - \log_{10} \frac{n_{X,\odot}}{n_{\text{Fe},\odot}},$$

where n_X denotes the absolute or relative abundance of element X and $n_{X,\odot}$ the corresponding solar abundance. The latter is somewhat uncertain; here we use the abundances from Magg et al. (2022).

2.2 Time scales in chemical evolution

Tinsley's concept of abundance planes relies on the fact that different progenitor types like core collapse SN, SNIa, neutron star merger, AGB stars, etc., have both different typical timescales and different abundance patterns in their ejecta, see e.g. Rauscher & Patkos (2010); Nomoto et al. (2013). We illustrate the main processes in Figure 1.

2.2.1 Elemental production with different timescales

Massive stars ending in core collapse supernovae (ccSN) are the main producers of α -elements like O, Ne, Mg, and contribute a major fraction of the Galactic iron peak elements around ^{56}Fe (Hoyle 1954). Before the supernova explosion, these massive stars ($\gg 10 M_{\odot}$) develop an onion-like structure with more progressed and hence heavier burning regions in the centre. Depending on how much of their envelopes are stripped before the supernova (up to being Wolf-Rayet-stars, Crowther 2007), they are classified as SNII (hydrogen

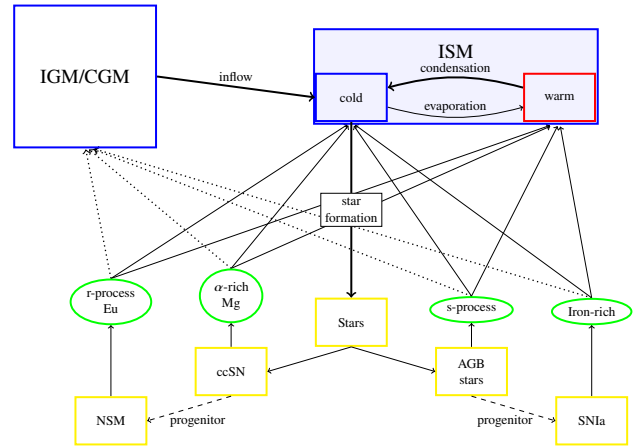


Figure 1. Diagram of the gas flows and enrichment processes in a Galaxy.

lines) and SNIb,c (no hydrogen lines, with/without helium), collectively called core collapse supernovae¹. The high mass drives fast nucleosynthesis, exhausting the stellar fuel at of order tens of Myrs and making enrichment with α -elements like Mg (magnesium) the fastest enrichment process.

Massive stars in multiple systems can leave behind tight neutron star binaries. When these merge, the ejected matter decompresses and undergoes r-process nucleosynthesis, where at extremely high neutron fluxes, neutrons are rapidly captured, before dropping to the neutron drip line in a series of beta-decays, producing elements like Au, U, Th, Gd, Eu, etc. (Burbidge et al. 1957). While other sites (e.g. collapsars) may contribute, it has been shown in Schönrich & Weinberg (2019) and Fraser & Schönrich (2021) that neutron star mergers (NSM) are the dominate r-process production site. As neutron star binaries require time for the inspiral (too small initial separation will likely be disfavoured due to the problem of inspiral in common envelope evolution), the NSM time delay distribution resembles the known SNIa time delay distribution with about an order of magnitude shorter timescales. Here we use a delayed onset time of 20 Myr and a decay distribution of $e^{-t/300\text{Myr}}$.²

At lower neutron fluxes than the r-process, the s-process contributes most elements between iron and lead. It likely does take place in (rotating) massive stars (Pignatari et al. 2008; Frischknecht et al. 2012), but the majority is found to stem from intermediate stars in their AGB phase (Clayton et al. 1961). Particularly, elements with "magic" neutron numbers in the valley of stability are produced by the s-process (e.g. Pb). Those have a corresponding peak of r-process elements (e.g. near Au) at lower nucleon numbers, due to the different neutron to proton ratio at which r- and s-process yield a magic neutron number isotope (Sorlin & Porquet 2008). While we do not explicitly track s-process elements in this paper, our evolution model does fully incorporate yields from low to intermediate mass stars. Beyond their s-process contribution, they contribute helium enrichment and larger amounts of otherwise unenriched yields at higher

¹ We do not differentiate exotic types here like symbiotic massive systems, electron capture supernovae or hypernovae

² This delay time is at the upper end of the currently expected range, Hotokezaka et al. (2018) e.g. uses $e^{-t/150\text{Myr}}$. However, it does not affect any of the qualitative claims made in this paper. Specifically, the effect is mostly one of temporal separation between ccSN and NSM and, seen in section 4, will mostly show as a shift of peak Eu production towards the inside of the nuclear ring.

population ages and hence are an important source of low-metallicity gas.

Finally, the majority of iron peak elements are produced by white dwarfs (WDs) exploding as SNIa (Thielemann et al. 1986). There are many possible channels for SNIa: classic single degenerate scenarios where an accreting CO WD exceeds the Chandrasekhar mass at $\sim 1.38 M_{\odot}$ (Chandrasekhar & Milne 1931; Whelan & Iben 1973; Nomoto et al. 1984), mergers/collisions (double degenerate scenario, e.g. Iben & Tutukov 1984, 1987), induced explosion by a helium nova on the surface (Fink et al. 2010; Kromer et al. 2010; Jiang et al. 2017), etc. Likely, all channels contribute (see e.g. Wang & Han 2012; Livio & Mazzali 2018; Soker 2018). We can afford agnosticism on this issue, as chemical evolution relies mainly on the feedback time. Here we assume standard yields from Iwamoto et al. (1999) and after an initial delay time of 0.45 Gyr we explode the SNIa on two exponential delay distributions, where a very small fraction of currently 1% follows a short time scale with $e^{-t/100\text{Myr}}$ and 99% a longer decay time of $e^{-t/1.5\text{Gyr}}$. We also note that the progenitor stellar remnants, i.e. the white dwarfs from ccSNe and neutron stars from AGB-stars, are already included in our scattering framework, before their final nucleosynthesis stage as SNIa and NSM. This ensures that those yields are significantly more dispersed than the ccSN yields that closely follow the radius of their initial formation.

2.2.2 Different gas phases

Another enrichment delay comes from the two-phase nature of the ISM. Most chemical enrichment models make the simplifying assumption of one gas phase. Contrasting with this, ISM models often distinguish three or more phases (see e.g. Ferrière 2001). However, it is well-established that galaxies are surrounded by hot circumgalactic medium (CGM), that most SN yields are initially in the hot phase (see e.g. the crab nebula), and that the hot ISM is cooling down slowly to feed the cold star-forming ISM on a timescale of ~ 1 Gyr. Most importantly, observations show both warm winds and chimney-like structures emanating from discs by which the hot-phase yields from SN escape from the disc plane (e.g. Krause et al. 2021). While this two-phase ISM was originally placed in the Schönrich & Binney (2009) models just as another free parameter, our later studies have shown that the time-delay plays an essential role in inverting disc metallicity gradients (see e.g. Spagna et al. 2010; Schönrich & McMillan 2017). Most importantly, the delay from the hot ISM directly resolves the r-process enrichment problem, as different splitting of yields into the cold vs. hot gas phases can effectively invert the time-delay relationship between r-process elements from NSM and α -elements from ccSN (Schönrich & Weinberg 2019). This study resolved the stark conflicts between chemical evolution models and observational evidence for neutron star mergers (Côté et al. 2018, 2019; Chornock et al. 2017), if the fraction of NSM yields injected into the cold phase is a factor ~ 2 larger than the fraction of ccSN yields. This argument was further sharpened by Fraser & Schönrich (2021). While there are good reasons to expect different fractions (NSM are spatially and temporally less correlated with the energetic outflows from ccSN that eject material far from the star-forming regions, and the heavy elements they yield cannot commonly be ionized in the hot ISM leading to faster cooling), the exact splitting into different phases lacks independent measurement paths, especially in the outer Galactic disc with its fairly continuous star formation.

2.3 Nuclear Discs

Like the majority of disc galaxies, the Milky Way possesses a central Galactic bar dominating the inner ~ 4 kpc. Due to the heavy obscuration of the Galactic central regions, this bar was first inferred from gas motions/radio observations (Johnson 1957). However, due to heavy dust obstruction, it has remained hidden for a long time and has only been widely accepted about 20 years ago through extended studies on radial gas inflow (e.g. Fux 1999; Englmaier & Gerhard 1999) and closer examination of the Galactic bulge that extends over the disc (Stanek et al. 1994; Binney et al. 1997). More recently, the stellar bar was clearly identified by its boxy/peanut shape (McWilliam & Zoccali 2010; Nataf et al. 2010).

Bars naturally form in most galaxies. As a disc galaxy rotates differentially the resonances move further outwards as the bar slows down in its formation process. However, even between the resonances, the orbits are shaped by the bar potential and their orientation with respect to the long axis of the bar changes. It can be shown (see e.g. chap. 3.3 Binney & Tremaine 2008) that inside the inner Lindblad resonance (ILR), the stellar orbits (so-called x_2 -orbits) are anti-aligned with the bar, while the bar itself is formed (amongst other orbit families) by the elongated x_1 -orbits between the ILR and the co-rotation resonance. This also poses a constraint to the possible length of the bar, as the orbits further out are again anti-aligned with the bar. Indeed, there are some reports about an inner ring in the Milky Way hypothesized to be formed by those orbits just outside co-rotation (Wylie et al. 2022).

As the bar sweeps through the gas in the galactic disc, it creates long shock lanes along its leading edges and tips (see e.g. fig. 3 of Athanassoula 1992). This gas falls on the leading side of the bar into the central region and accumulates on the dense nuclear disc (on x_2 orbits, Contopoulos & Grosbøl 1989). Turbulence and shear suppress star formation in the bar lanes, so they can be modelled in chemical evolution as direct infall from the bar tips. The inflow speed is of order $\gtrsim 100 \text{ km s}^{-1}$, as found e.g. by Sormani et al. (2023) for NGC 1097.

Predicting the size of a nuclear disc is difficult. Historically, it was only known that the ILR poses an outer limit (see e.g. Simkin et al. 1980; Combes & Gerin 1985; Buta & Combes 1996). Recently, advances have been made here, taking e.g. the viscosity/sound speed of the gas into account (van de Ven & Chang 2009; Sormani et al. 2018). The full picture however remains unclear.

The radius at which the inflowing gas settles in the galactic centre is referred to as nuclear ring (for the Milky Way: the central molecular zone (CMZ)). Due to the strongly increased gas density in this region, the nuclear ring vigorously forms stars (up to 5% of its galaxy's star formation; Kennicutt et al. 2005). These rings were observed (Knapen et al. 1999; Comerón et al. 2010) before being shown to be just the outer edge of inside-out forming, i.e. radially growing nuclear stellar discs (Bittner et al. 2020), now corroborated by the detection of a consistent radial age gradient (Nogueras-Lara et al. 2023b). We thus concentrate on inside-out forming nuclear disc models in this paper.

A consistent gas supply is ensured by the deceleration of the galactic bar, due to loss of angular momentum to the dark halo (see e.g. Debattista & Sellwood 2000; Berentzen et al. 2007; Dubinski et al. 2009). This slow-down moves the bar resonances outwards and hence also the radius from which the bar funnels material to the centre. This deceleration has been proven in solar neighbourhood kinematics recently (Friske & Schönrich 2019; Chiba et al. 2020; Chiba & Schönrich 2021), which also allowed for a precise measurement of the bar pattern speed and corotation resonance radius ($R_{CR} = 6.6 \pm 0.2 \text{ kpc}$).

The outward shift in the feeding radius (expected to be linear in time in simulations; see e.g. Fig.2 [Aumer & Schönrich 2015](#)) strongly affects the composition of funnelled-in central gas. We will discuss this in [section 4](#).

Finally, we note that despite its interest, the nuclear disc is the most understudied region in the Milky Way. Due to the heavy dust obscuration ($\gtrsim 3$ mag in the infrared K-band, completely blacking out the V-band), the identification of the CMZ ([Rougoor & Oort 1960](#); [Petters 1975](#); [Banja 1977](#); [Liszt & Burton 1978](#); [Bally et al. 1988](#)) (as slowly pieced together as it was) predated the stellar observation in first density and then kinematics ([Launhardt et al. 2002](#); [Schönrich et al. 2015](#)) by nearly half a century. To date, detailed and reliable abundance information for the Galactic nuclear disc is scarce (see also the Appendix). We also note that the relationship between the nuclear star cluster (~ 100 times smaller) and the nuclear disc, in particular the contribution of later-formed nuclear disc stars to a pre-dating nuclear star cluster is unknown and we will leave discussion to future study.

It is important to discern the nuclear disc from other strongly light-emitting objects at the centre of galaxies, especially from the inherently older classical bulges or x-shaped bars, which are either caused by (recurrent) bar buckling ([Athanasoula & Misiriotis 2002](#); [Martinez-Valpuesta et al. 2006](#); [Fragkoudi et al. 2019](#)), or secular processes ([Sellwood & Gerhard 2020](#)). In contrast to this, nuclear disc stars form after the creation of the bar (see [Baba & Kawata 2020](#), for a discussion) in situ in the nuclear disc. In contrast to classical bulges, nuclear discs will have much stronger rotational support and likely colder kinematics.

We note that a small number of nuclear discs have been detected in non-barred galaxies (see e.g. the AINUR catalogue [Comerón et al. 2010](#)). However, these are rare, comparably faint, and might result from merger events ([Mayer et al. 2008](#)), and/or destruction of their host bars. We leave these to later study.

2.4 Chemical Compositions of Nuclear Discs in the Literature

As mentioned above, our in-disc position hampers observations of the MW's nuclear disc. It is hence beneficial to study other galaxies, that, with high-enough inclination provide a spatially resolved view. Currently, studied nuclear discs tend to be larger (500 pc vs. our ~ 150 pc) and more dominant in mass and luminosity.

The Calar Alto Legacy Integral Field Area Survey (CALIFA) has spectroscopically mapped ~ 600 local/low- z galaxies. [Sánchez-Blázquez et al. \(2014\)](#) studied the bar influence in 62 face-on spiral galaxies. Some of these show a nuclear disc; however, the resolution is not sufficient to spatially dissect the nuclear discs and quantitatively compare with the bar tips. CALIFA has also only studied metallicity and not detailed abundance ratios.

The BaLROG (Bars in Low Redshift Optical Galaxies) sample taken with the Spectrographic Areal Unit for Research on Optical Nebulae (SAURON, William Herschel Telescope, Observatorio del Roque de los Muchachos, La Palma; [Bacon et al. 2001](#)) comprises 16 large mosaics of barred galaxies. [Seidel et al. \(2016\)](#) calculate ages, metallicities and [Mg/Fe] abundance ratios mapping their gradients along the bar major and minor axes. Again, the spatial resolution precludes definitive conclusions; however, visual inspection comparing the nuclear disc abundances to the abundance at the bar tips at least suggests a correlation.

Explicitly dedicated to nuclear discs and rings is the TIMER (Time Inference with MUSE in Extragalactic Rings) sample of 21 barred spiral galaxies taken with the MUSE (Multi Unit Spectroscopic Explorer) integral field spectrograph ([Gadotti et al. 2020](#)). [Bittner et al.](#)

(2020) corroborated the idea of an analogous inside-out formation of nuclear discs to ordinary galactic discs and of nuclear rings as the most recent place of gas accretion and star formation at the rim of their nuclear disc. They also observe enhanced α -enrichment in nuclear rings. However, their observations do not reach out to the ends of the host bars, precluding a direct determination of the nucleosynthesis within the nuclear disc vs. accretion of pre-enriched material.

Also using MUSE, the PHANGS (Physics at High Angular resolution in Nearby Galaxies)-MUSE survey ([Emsellem et al. 2022](#)) studies 19 galaxies, most of which harbour nuclear discs. The first data release did not yet provide reliable metallicities. (A first study, deriving metallicities ([Groves et al. 2023](#)) showed global metallicity variations, however from $H\alpha$ emitting, ionised nebulae that are not well-resolved within the nuclear disc.) When future data releases include detailed abundances, we expect these data the best route to constrain our models.

Looking back at our own Galaxy, the Apache Point Observatory Galactic Evolution Experiment (APOGEE, see [Majewski et al. 2017](#)) has a few pointings in the Galactic centre. The latest and final data release DR17 ([Abdurro'uf et al. 2022](#)) contains spectra for 43,200 bulge stars. A unique nuclear disc selection is difficult, but using a reddening cut $A_K > 3.0$ mag yields ~ 300 very bright, but cool ($T < 3600$ K) giant stars. However, while the spectra look promising for a dedicated analysis, using the prederived stellar parameters, only 113 stars with published metallicities pass the recommended quality cuts, and those show generally low metallicities (down to $[Fe/H] \sim -1.2$ and one outlier at $[Fe/H] \sim -2.5$), which seems very low and strangely distributed compared to e.g. the KMOS NSD sample discussed below. (See a comparison in [Figure A2](#)).

Recently, major advances are made using the K-band Multi Object Spectrograph (KMOS; [Sharples et al. 2013](#)) operating on the VLT that is specifically designed for integral field spectroscopy at high reddening. [Fritz et al. \(2021\)](#) obtained for the first time spectroscopic metallicities for ~ 3000 nuclear disc stars, obtained by [Feldmeier-Krause et al. \(2017\)](#), again mostly targeting tip-AGB stars, so age and metallicity selection biases will have to be taken into account. [Schultheis et al. \(2021\)](#) used this data for a first study of metallicity gradients in the Galactic nuclear disc. They found that the nuclear disc is likely made up by a larger, kinematically cold, rotating metal rich population and a smaller, partially even retrograde metal poor sample, with likely different origin. They measured a vertical gradient, which they suspect to be due to vertically increasing contamination with bulge stars. They found no significant radial metallicity gradients; however, the strong favouring of the nuclear ring by sample selection and dust obscuration is not yet accounted for. Very recently, ([Nogueras-Lara et al. 2023a](#)) connected those to photometric data and indeed found a negative metallicity gradient consistent with extragalactic results e.g. in [Bittner et al. \(2020\)](#).

3 MODEL

3.1 General Model

We use a newly implemented variation of the chemical evolution models from [Schönrich & Binney \(2009\)](#), with added inside-out formation ([Schönrich & McMillan 2017](#)) and the hot/cold gas phase calibrations from ([Schönrich & Weinberg 2019](#)). The code will be published separately, but can already be retrieved.³ We describe here

³ https://github.com/DrFraserGovil/RAMICES_II

simulation time/ age	12 Gyr
step size	10 Myr
galactic disc ring number	100
galactic disc ringwidth	0.2 kpc
total mass at start (M_0)	$10^8 M_\odot$
final scalelength (R_f)	4 kpc
early infall mass (M_1)	$40 \times 10^9 M_\odot$
early infall timescale (b_1)	1 Gyr
long infall mass (M_2)	$100 \times 10^9 M_\odot$
long infall timescale (b_2)	9 Gyr

Table 1. Main Simulation parameters for the global galactic simulation. The definition for the infall is the same as in equation 2 of Schönrich & Binney (2009).

nuclear disc ring number	50
nuclear disc ringwidth	3 pc
$f_{c,ccSN}$	0.2
$f_{c,NSM}$	0.4
$f_{c,AGB}$	0.3
$f_{c,SNIa}$	0.01
global eject fraction	0.55
nuclear eject fraction	0.65
total mass at start	$10^6 M_\odot$
final scalelength	70 pc

Table 2. Average Model parameters

the main elements relevant for modelling the nuclear disc in our new adaptation. Table 1 lists the main set-up parameters used throughout this paper.

The simulation uses (time-dependent) disc scalelengths (see below), total stellar mass ($\sim 5 \times 10^{10} M_\odot$), and total age (12 Gyr) comparable to the Milky Way. With timesteps of 10 Myr, it resolves 100 concentric rings (width 200 pc), which yields sufficiently small abundance differences between neighbouring rings (~ 0.01 dex).

We use a Chabrier initial mass function (IMF) (Chabrier 2003). With the difference to e.g. Salpeter’s IMF mostly on low-mass stars, the IMF choice mostly results in moderate equilibrium metallicity differences, which are degenerate with mass loss parameter. Star formation rates (SFR) are determined with a Kennicutt-Schmidt law (Kennicutt 1998; Schmidt 1959): Star formation efficiency rises at higher gas surface density, with a cut-off at low density where the gas becomes stable against gravitational collapse. This is important especially in a region like the NSD with high gas density variations. We note that it is likely that magnetic fields (e.g. Moon et al. 2023) and turbulence (Nesvadba et al. 2011; Longmore et al. 2013) change the SFR in the NSD and specifically in the CMZ.

3.2 ISM, gas flows

The multi-phase ISM is implemented as a hot and a cold (star forming) reservoir. The different contribution of each feedback source X to the cold gas phase are listed in Table 2, as $f_{c,X}$; they are chosen consistently with Schönrich & Weinberg (2019), such that $f_{c,NSM}/f_{c,ccSN} \sim 2$ and the remaining freedom is used to improve the match to the local abundance gradients. The proposed values should only be seen as a starting point for future analysis.

The initial galactic gas disc only contains primordial, cold gas with total mass $10^8 M_\odot$ as 76% hydrogen and 24% helium. The disc forms inside-out with a growing gas scalelength (Figure 2) that settles at 3.77 kpc at the upper end of current observations (Kalberla & Dedes 2008).

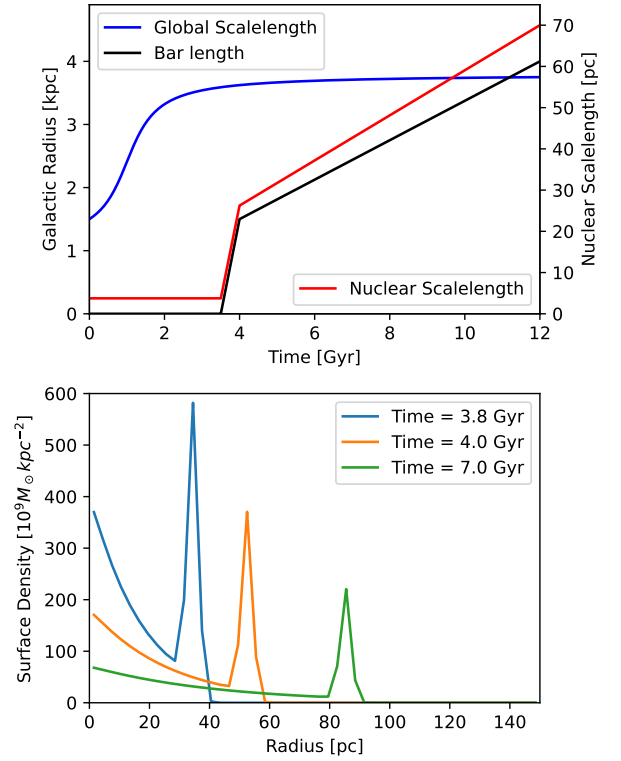


Figure 2. Top: Evolution of the scalelength of the gaseous disc over simulated time

Bottom: Shape of the gas distribution in the nuclear disc at different times

Following Schönrich & Binney (2009) we parametrise the gas onfall with two exponential functions in time, one fast component driving the initial build-up of the disc and the slower term guiding the long-term decline in star formation, keeping the parameters identical to Schönrich & McMillan (2017) apart from lowering the fast onfall mass to $40 \times 10^9 M_\odot$ (see Table 1). The formalism approximates gas accretion via the hot galactic corona (see Lacey & Fall 1985): Due to the corona’s thermal pressure support, the onfalling gas has a lower specific angular momentum ($\sim (2/3)v_c$ to $(3/4)v_c$) than the disc gas ($\sim v_c$); thus accretion dilutes disc angular momentum, driving a continuous radial inflow. Secondly, Lacey & Fall (1985) argued that friction in the viscous gas layers works towards equilibrating the angular rotation speed of the gaseous disc and results in a gain of angular momentum in the outer parts and a loss and hence an inflow motion in the inner parts of the galaxy. While it is unclear how important this effect is for large scale galactic discs, it will likely be much more relevant for the small, turbulent and quite magnetised nuclear discs. Portinari & Chiosi (2000) argued that a galactic bar not only shapes the chemical evolution in the area it sweeps over, but impacts the global metallicity gradient and gas profile as it quickly takes up gas around its tips and efficiently funnels it towards the centre. Lastly, large scale structures such as spirals and bars drive angular momentum exchange and inflow. In total, the resulting flows determine the global metallicity gradient (Lacey & Fall 1985; Goetz & Koeppen 1992). Here, we model gas inflow and onflow with the recipe of Bilitewski & Schönrich (2012), which couples radial inflow, onfall and their radius-dependent ratios by balancing their angular momentum.

Some gas is expected to leave the galactic disc region: we assume that in each supernova, NSM, etc., a fraction of the yields is directly ejected to the CGM (we call it galactic disc ejection fraction in this

paper). This ejection fraction affects overall metallicity and chemical evolution timescales, and we do a preliminary test in section [4](#).

3.3 Modelling bar and nuclear disc

3.3.1 Profiles and accretion

The simulation setup is intrinsically axisymmetric, but the main effect of a bar on chemical evolution is included by the radial gas flows it evokes, namely, wiping out the gas disc in the bar region, funneling gas from the bar tips into the central region, and building up a nuclear disc with high density and rapid star formation.

In our code we model this new nuclear disc as a second disc model with 50 rings of width 3 pc, i.e. a total covered extent of 150 pc. This disc starts with negligible mass; once the bar forms, the nuclear disc quickly receives the cold gas present within the bar radius, with a maximum transport efficiency of 50%. After this, the bar length grows linearly and the main disc gas reached by the growing bar radius is added onto the nuclear disc.

To determine the distribution of onflow onto the nuclear disc, we fix the shape of its gas surface density. We set a two-part structure with equal mass in the exponential disc of scalelength $R_{\text{ND}}(t)$, and a nuclear ring at $r_{\text{NR}}(t) = 2R_{\text{ND}}(t)$ (i.e. nuclear ring fraction $f_{\text{NR}} = 0.5$) with a Gaussian width $\sigma_{\text{NR}} = 0.35 \times 5$ pc, and followed at $r > R_{\text{NR}}(t) + 5$ pc by a steep cut-off (communicated by $\delta_{\text{cut-off}}$) with exponential scale 1 pc.

$$\begin{aligned} \Sigma(r, t) &= (1 - f_{\text{NR}}) \times \Sigma_{\text{Disc}} \times \delta_{\text{cut-off}}(r, t) + f_{\text{NR}} \times \Sigma_{\text{NR}} \quad (1) \\ \Sigma_{\text{disc}}(r, t) &= \Sigma_0 \exp\left(-\frac{r}{R(t)}\right) \\ \Sigma_{\text{NR}}(r, t) &= \frac{\Sigma_0}{\sigma_{\text{NR}} \sqrt{2\pi}} \exp\left(-\frac{(r - r_{\text{NR}})^2}{2\sigma_{\text{NR}}^2}\right) \\ \delta_{\text{cut-off}}(r, t) &= \begin{cases} 1 & r < r_{\text{NM}} + \Delta_{\text{NR}}/2 \\ \exp\left(-\frac{r - (r_{\text{NM}} + \Delta_{\text{NR}}/2)}{1 \text{ pc}}\right) & r \geq r_{\text{NM}} + \Delta_{\text{NR}}/2 \end{cases} \end{aligned}$$

where the scalelength as a function in time is

$$R_{\text{ND}}(t) = \begin{cases} R_{\text{ND},0} & t < t_{\text{bar}} \\ R_{\text{ND},0} + \frac{t - t_{\text{bar}}}{t_i} (R_{\text{ND},i} - R_{\text{ND},0}) & t_{\text{bar}} < t < t_{\text{bar}} + t_i \\ R_{\text{ND},i} + \frac{t - (t_{\text{bar}} + t_i)}{t_{\text{total}} - (t_{\text{bar}} + t_i)} (R_{\text{ND},f} - R_{\text{ND},i}) & t > t_{\text{bar}} + t_i \end{cases} \quad (2)$$

Here $R_{\text{ND},0}$ is the starting scalelength at bar formation ($t_{\text{bar}} = 3.5$ Gyr), $R_{\text{ND},i}$ the scalelength of the nuclear disc at the end of the initial growth phase, and $R_{\text{ND},f}$ the final scalelength (see [Figure 2](#)). The bar length follows the analogous equations:

$$r_{\text{bar}}(t) = \begin{cases} 0 & t < t_{\text{bar}} \\ \frac{t - t_{\text{bar}}}{t_i} r_{\text{bar},i} & t_{\text{bar}} < t < t_{\text{bar}} + t_i \\ r_{\text{bar},i} + \frac{t - (t_{\text{bar}} + t_i)}{t_{\text{total}} - (t_{\text{bar}} + t_i)} (r_{\text{bar},f} - r_{\text{bar},i}) & t > t_{\text{bar}} + t_i \end{cases} \quad (3)$$

where $r_{\text{bar},i} = 1.5$ kpc is the length of the bar after the initial growth phase and $r_{\text{bar},f} = 4$ kpc the final bar length. With these definitions, the inner part of the NSD has a comparably low gas density at the end, dwarfed by the nuclear ring gas density. This is consistent with findings that the majority of the NSD extinction happens at the nuclear ring at the outer edge, while the nuclear disc itself accounts only for about 10% of the total extinction ([Nogueras-Lara 2022](#)).

We make the assumption that the nuclear disc inflow inherits the abundance at the bar tips. For this, all cold gas at the expanding bar length is put into a reservoir (which may be thought of as the infall lanes) and immediately transferred it onto the nuclear disc conserving the density profile above. The surface density of the nuclear disc gas at different times is shown in the lower panel of [Figure 2](#).

3.3.2 Transport within the nuclear disc

Some nuclear discs are known to exhibit substructures (particularly spirals) similar to large galactic discs (e.g. [Maciejewski et al. 2002](#); [Erwin 2004](#)), and so both radial transport and stellar migration can be expected. Those substructures seem to be more prevalent in larger discs. To elucidate the consequences, and to cope with our lack of understanding how material flows within nuclear discs, we here consider two opposing scenarios:

The first one (the "onfall" scenario) achieves the surface density in [Equation 1](#) solely by onflow from the galactic disc. I.e., apart from a small blurring effect due to increased eccentricity of older stars, no stars or gas is exchanged between different rings of our model.

This is contrasted by our "inflow" model, where the onfall is restricted to the area of the nuclear ring. The rest of the gas surface density is sustained by subsequent inflow through the nuclear disc.

We cap this inflow between neighbouring rings at each timestep at 10% of the available mass (or about 0.3 km s^{-1}). This means that it is possible that the prescribed surface density in [Equation 1](#) is not achieved. The gas mass in the inflow scenario is on average half as high than the infall scenario, which also leads to an average star formation efficiency half as high as the the onflow scenario (compare [Figure 3](#)).

No knowing how much blurring or churning the nuclear disc should have, we conduct this experiment with these terms heavily suppressed in either scenario. These can be measured once detailed stellar abundances and phase space information are known.

We will later see that while the formation scenario strongly influences the radial abundance profile in the nuclear disc, the global effect of the different gas parameters stays (mostly) the same.

The nuclear disc has a comparably small circular velocity $v_c \sim 125 \text{ km s}^{-1}$, the system fills a quite small volume, and there is plentiful heating from the high rate of SNe. Together with the observations of outflow above the nuclear disc, this leads to the assumption that the nuclear disc cannot retain the majority of the hot ISM produced there. Here, we encode this by expelling 10% of the present hot gas in each 10 Myr time step (i.e. a residence timescale of ~ 100 Myr which is an order of magnitude smaller than the gas cooling time).

On more possible gas accretion has to be considered: onfall from the galactic corona onto the nuclear disc. As mentioned above, this accretion is poorly understood observationally and theoretically in the outer disc, and there is currently no prediction if this happens at all in the very centre. The nuclear disc is surrounded on both sides by the two Fermi bubbles (which may be driven by AGN eruptions and/or the nuclear disc winds, first reported in [Bland-Hawthorn & Cohen 2003](#), see further [Su et al. 2010](#); [Dobler et al. 2010](#); [Yang et al. 2018](#)). These likely shield the nuclear disc against onfall. While they seem to be transient, it is likely that similar outflows prevail for most of the time above the nuclear disc. Furthermore, the strongly star forming nuclear ring likely also drives outflows, preventing accretion of coronal gas. We hence do not include direct onfall from the CGM in our models. However, even if present, onfall from the Corona would reduce the overall metallicity, but is not expected to affect abundance ratios.

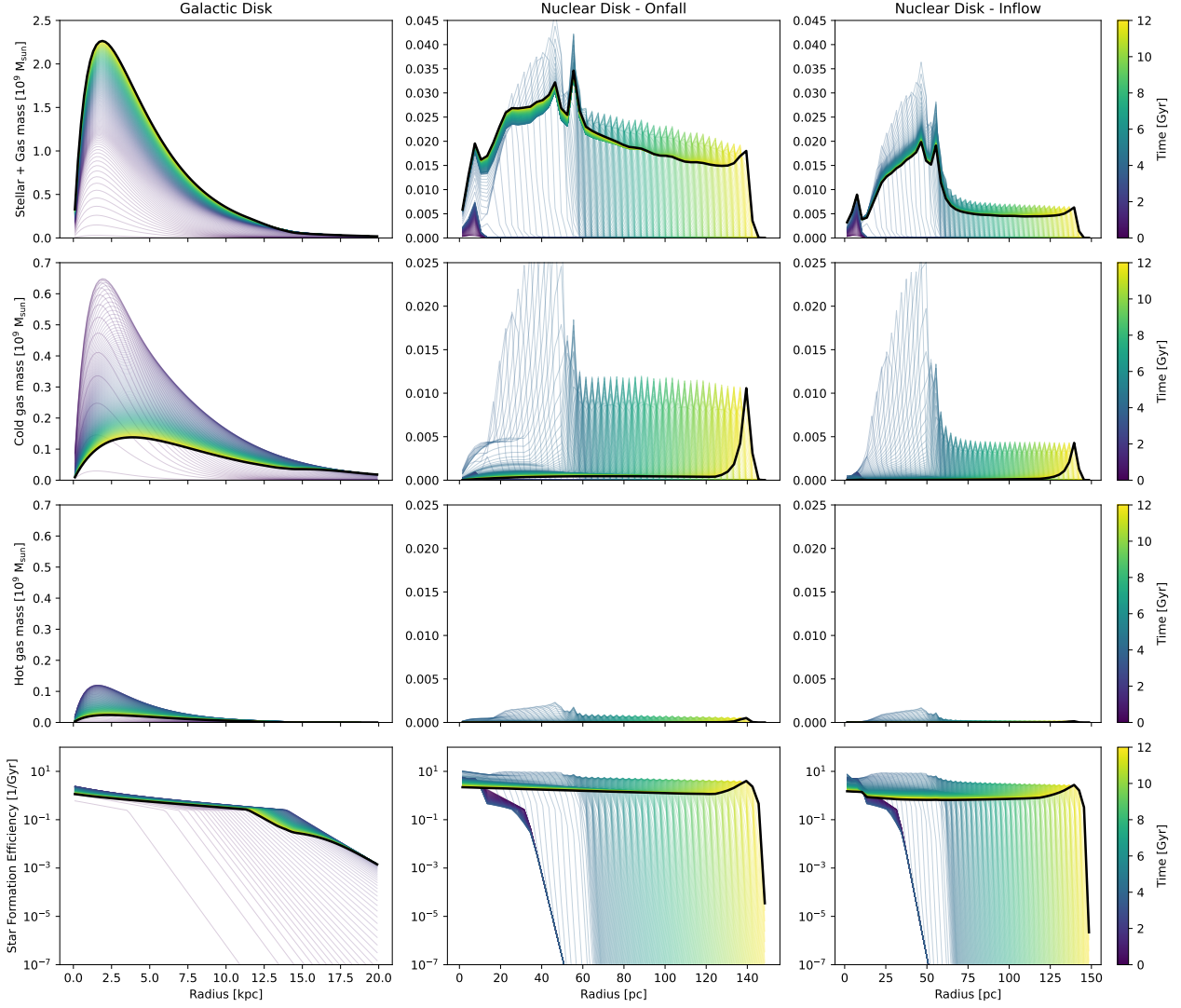


Figure 3. Total (i.e. stellar and gas) mass, mass of the cold and hot gas and star formation efficiency for the total galactic disc (left column) and the nuclear disc for both of our accretion scenarios (right two columns). The thick black line in every case shows the final mass/star formation efficiency profile.

Flows within the nuclear disc can currently not be constrained by the angular momentum balance with respect to the corona, the gas funnelled by the bar, nor is it clear how angular momentum is transferred within the nuclear disc. [Sormani et al. \(2023\)](#) measured the inflow velocity onto the nuclear disc in NGC 1097, but that does not resolve the question how much angular momentum this gas transfers onto the nuclear disc.

As in the general disc, the nuclear disc also loses a large fraction of its gas yields to the CGM. Due to its small vertical and radial extent and low angular momentum it is likely that this nuclear ejection fraction (EF_{nuc}) is significantly higher than the galactic disc EF, but even more difficult to directly measure. We nevertheless expect it to strongly affect the influence of the inflowing gas on the nuclear disc. Therefore, we study its effect on the NSD abundance in our models in [section 4](#).

3.4 Summary of gas flows

In summary we bracket the set of reasonable assumptions by our two main scenarios, setting the following assumptions on the gas flows:

No onfall from the corona/CGM. Similar hot/cold gas phase fraction in stellar yields as in the main galactic disc, but rapid gas loss from the hot phase. Stellar yields in the bar region and gas from the bar tips are directly funnelled onto the nuclear disc. Within the nuclear disc, we either a) add the funnelled gas onto the outer ring and allow for an inflow sustaining the inner nuclear disc (our favoured scenario), or b) add the funnelled gas directly onto each ring in the nuclear disc without radial flows.

4 RESULTS

4.1 Mass Evolution of the Nuclear Disc

First we examine the mass profiles over time in the nuclear disc. The top left panel of [Figure 4](#) shows the total (i.e. stellar + gas) mass per ring of the nuclear disc vs. time, while colour codes the radius. The top right and bottom left panels show the total and cold gas mass, while the bottom right panel displays the star formation efficiency. In our set-up, the innermost ring receives a small amount of gas

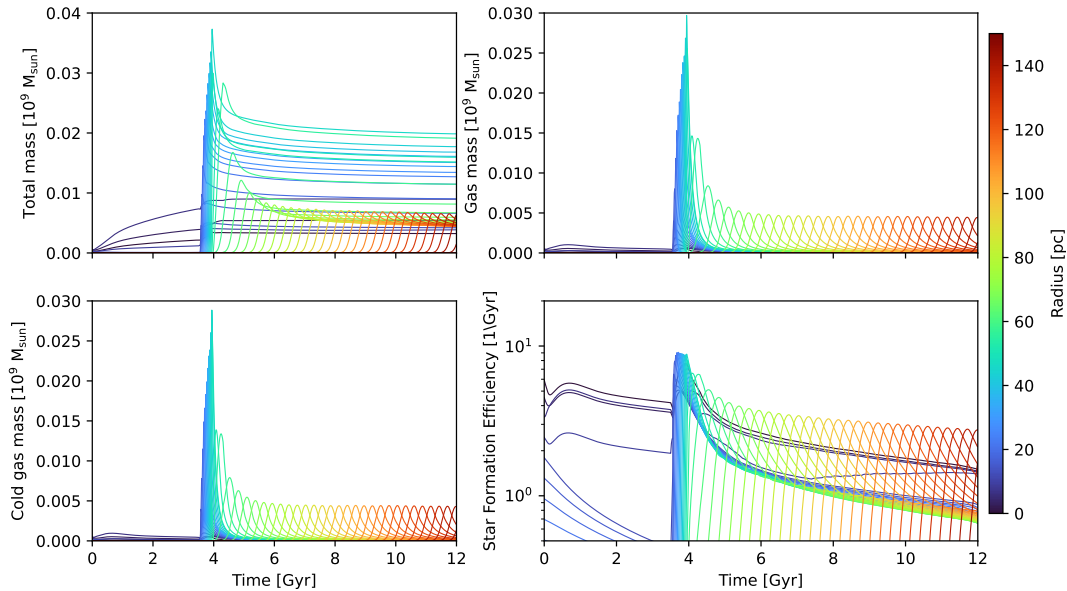


Figure 4. Total mass, gas mass, mass of the cold gas and star formation efficiency for the nuclear disc in the inflow scenario. The changing colours from blue to red correspond to increasing radius.

from the central galactic disc before bar formation, and blurring distributes some of this gas to the neighbouring rings. We note that this phase has virtually no effect on the results for the remainder of the simulation. During the initial bar formation around $t = 3.5$ Gyr, the gas mass peaks in the central region and drives a very strong and sustained star-formation burst with star formation efficiencies reaching up to $1/100$ Myr. This leads to a rapid build-up of mass in the inner rings. After this initial phase, the main star-formation site is the slowly expanding nuclear ring. While our model has continuous star formation, all our models show a short decrease in the stellar mass after the initial star-formation spike, when the high- and intermediate-mass stars from the burst die, followed by a slower subsequent build-up of mass. We note that while in this model the star-formation efficiency in the very central region still rivals that of the nuclear ring, this central region is small, and the ring dominates the star formation in the disc, consistent with the observation of the ring in relatively young tip-AGB stars in Schönrich et al. (2015), while the overall mass density peaks clearly in the centre as demanded by infrared photometry (e.g. Launhardt et al. 2002). The final mass in the onfall model is $9.6 \times 10^8 M_{\odot}$, which is consistent with the estimate of $M_{\text{NSD}} = 10.5^{+0.8}_{-0.7} \times 10^8 M_{\odot}$ from Sormani et al. (2022). We note that the inflow model stays below this at $3.8 \times 10^8 M_{\odot}$.

4.2 Abundance Profile in the Nuclear Disc

Before we vary single parameters, we examine the (observable) abundance patterns predicted in the nuclear disc at the end of the simulation for both the onfall and the inflow scenarios, shown in Figure 5 and 6. (The corresponding plots in [Eu/Fe] can be found in Figure A3, with an overall shape very similar to [Mg/Fe], and an analogous explanation, while swapping in NSM for ccSN.) The top row shows today's (i.e. at $t = 12$ Gyr) overabundance of each nuclear disc radius measured relative to the current bar tips near $R = 4$ kpc, from where the gas flows onto the nuclear disc. This means that a value of 0.1 dex e.g. for [Fe/H] in the top-left panel is not measured relative to the Sun, but means that that radius in the nuclear disc is 0.1 dex

or 25% more enriched in iron than the current star-forming gas at the bar tips. We make this choice to reduce the impact of nuisance parameters, like outer disc dynamics/history, and e.g. ejection rate parameters, which change the overall abundances, but say little about the nuclear disc. The relative measure should also be less biased in observations.

Comparing the top row in both scenarios, we see strong qualitative differences between the two scenarios driven in parts by the different star formation patterns and most importantly, by different gas flow patterns. There are three competing influences on the abundance of each ring in the inflow scenario (and two in the onfall scenario): i) the star-formation history and in-situ production of metals, ii) the time-dependent abundances of the funnelled gas from the outer disc, and in the inflow scenario also iii) the enrichment in the nuclear disc outside the current radius. The overall abundances of the gas funnelled inwards are given by the overall chemical evolution of the galactic disc: a relatively swift initial rise in metallicity at high α -element enrichment, which plateaus around the same time (of order 2-3 Gyr) as SNIa lower the α -abundances to solar values. Depending on its formation time, the nuclear disc will experience the tail end of this phase of increasing metallicity and decreasing $[\alpha/\text{Fe}]$. At later times, the change in infall composition is dominated by the radial abundance change due to the galactic metallicity gradient, as the bar reaches larger radii, i.e. the metal-content of the funnelled gas is expected to slowly decline.

The resulting patterns are best understood in two ways: i) by examining the trajectory in the abundance plane and hence the temporal evolution of single rings ii) by considering the relative star formation together with the change in gas (in)flows.

For the former we show the evolution of the very typical rings 18 (and 10 for the inflow scenario) in the abundance plane ([Mg/Fe] vs. [Fe/H]) in the bottom left panel of Figure 5 (and Figure 6 respectively) coloured by time since filling, i.e. since the nuclear ring has expanded to this radius. Each ring performs a clockwise loop in the abundance plane: With the initial star formation spike, both the overall metallicity and (to a lesser extent) [Mg/Fe] quickly rise, as first the ccSN enrich the star-forming nuclear ring with α -elements and

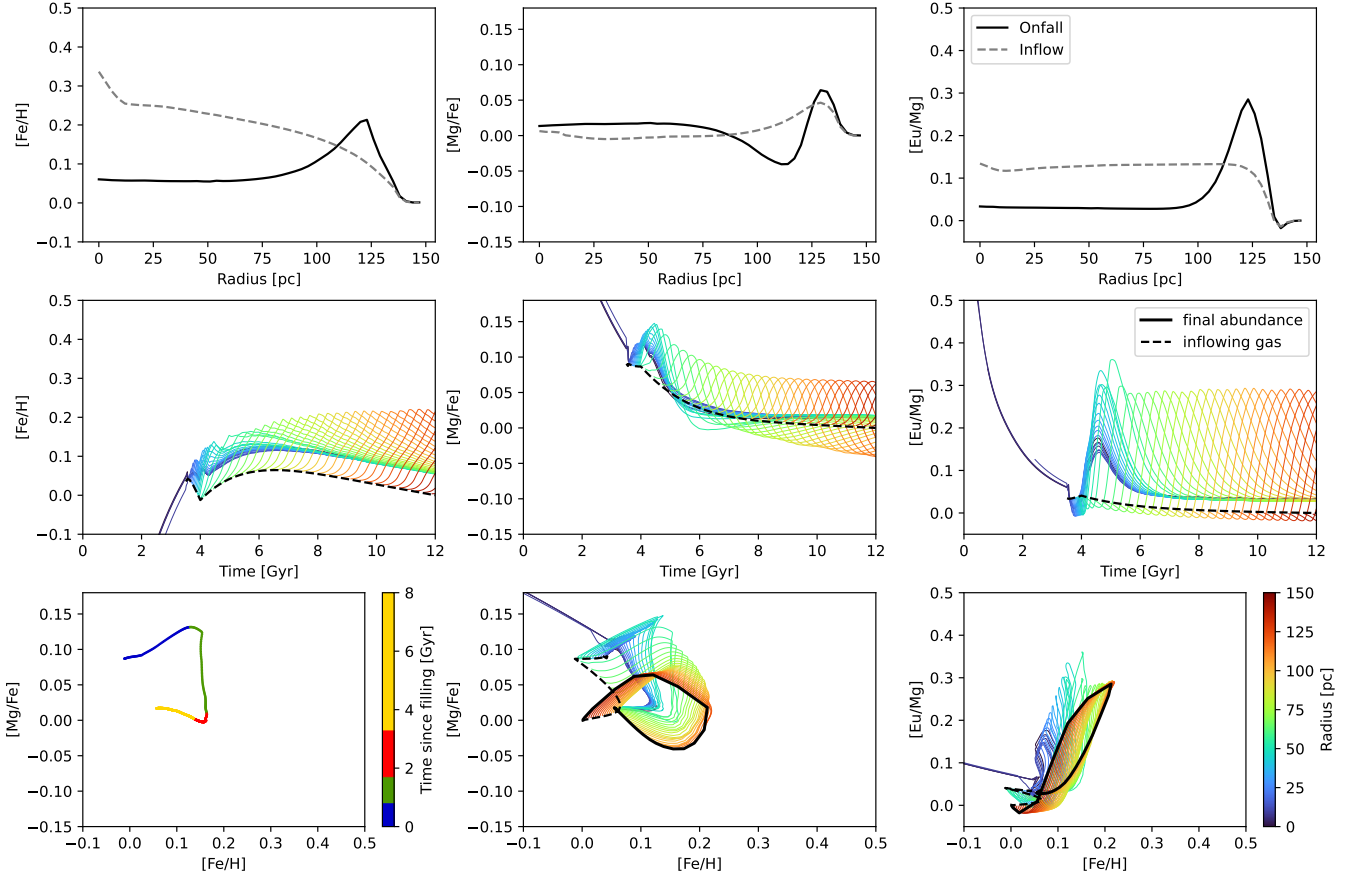


Figure 5. Onfall scenario: *Top row:* Gas overabundance profiles in the nuclear disc for Iron, [Mg/Fe] and [Eu/Mg] for our average model in the onfall scenario. The overabundance is calculated as difference between the abundance at each radius in the nuclear disc and the abundance just outside the gas depleted bar region. For comparison, we also show the abundance profile of our competing inflow accretion history.

Middle row: General evolution of the elemental overabundance in the cold gas over time. The lines following each ring are drawn once the mass of the ring exceeds $4 \times 10^6 M_{\odot}$. The dashed line shows the abundance of the accreted gas over time.

Bottom row: The panels in the middle and on the right give the relative abundance plane for magnesium and europium respectively. The final abundance is drawn in solid black and the abundance of the accreted gas as a dashed line. The leftmost panel shows again the magnesium abundance plane, however only for ring 18. The timescale is adjusted to start once this ring receives gas from the outer galaxy.

some iron. In the second phase (green), enrichment by SNIa kicks in, lowering the [Mg/Fe] ratio while still raising the [Fe/H] abundance. During this and the third phase (red) the star-formation peak and gas enhancement moves to the outside of the considered ring’s radius and the importance of in-situ metal production declines. Here, the two scenarios behave quite differently. In the onfall scenario, our ring stays supplied from the bar tips. As these move slowly outward in this galaxy with a negative metallicity gradient, the overall metallicity of the funnelled gas keeps slowly declining, directly driving a corresponding decline in the ring metallicity. In the inflow scenario all gas is delivered through the outer nuclear disc with its current star formation spike, so the gas reaching the ring is pre-enriched by the increasing width of nuclear disc on its outside, which compensates for some of the decline, especially in metallicity.

Let us now look at the time-evolution of all rings, shown in the middle row of both Figure 5 and 6. In the onfall scenario, the overall trends of the funnelled gas can be clearly seen in the dashed line: the initial rise in [Fe/H] is followed by a slow decline in the past ~ 6 Gyr. Similarly [Mg/Fe] shows a slow decline. As [Eu/Mg] traces the relative importance of NSM and ccSN, the very slow decline in [Eu/Mg] is a lingering effect of the larger $f_{c,NSM}$ which means that

more of the ccSN yields from early galactic star formation remain locked up in the hot ISM phase and only gradually cool on a Gyr timescale.

Starting from these main trends, we see the changes at each radius after it is reached by the expanding nuclear ring: an initial rise in [Fe/H], [Mg/Fe], [Eu/Mg] followed by a decline once the ring has passed. [Mg/Fe] first rises sharply and is then taken slightly below the inflowing abundance when the ccSN burn out and SNIa from the initial star formation peak dominate. Due to the shifted timescales of NSM and ccSN, [Eu/Mg] follows the inverse trend, exhibiting a dip first and then a rise when NSM dominate over ccSN, before eventually levelling out when the radius reaches equilibrium star formation. Again, due to the larger fraction of NSM yields being in the cold phase than ccSN, the rise is stronger than the dip. Similarly, we see in the bottom row that each radius initiates a clockwise loop around the main trend, while it is passed by the main nuclear ring.

4.3 Influence of the Gas Inflow History

It is instructive to analyse the differences between the onfall and inflow models. In the onfall scenario, rings are filled by directly

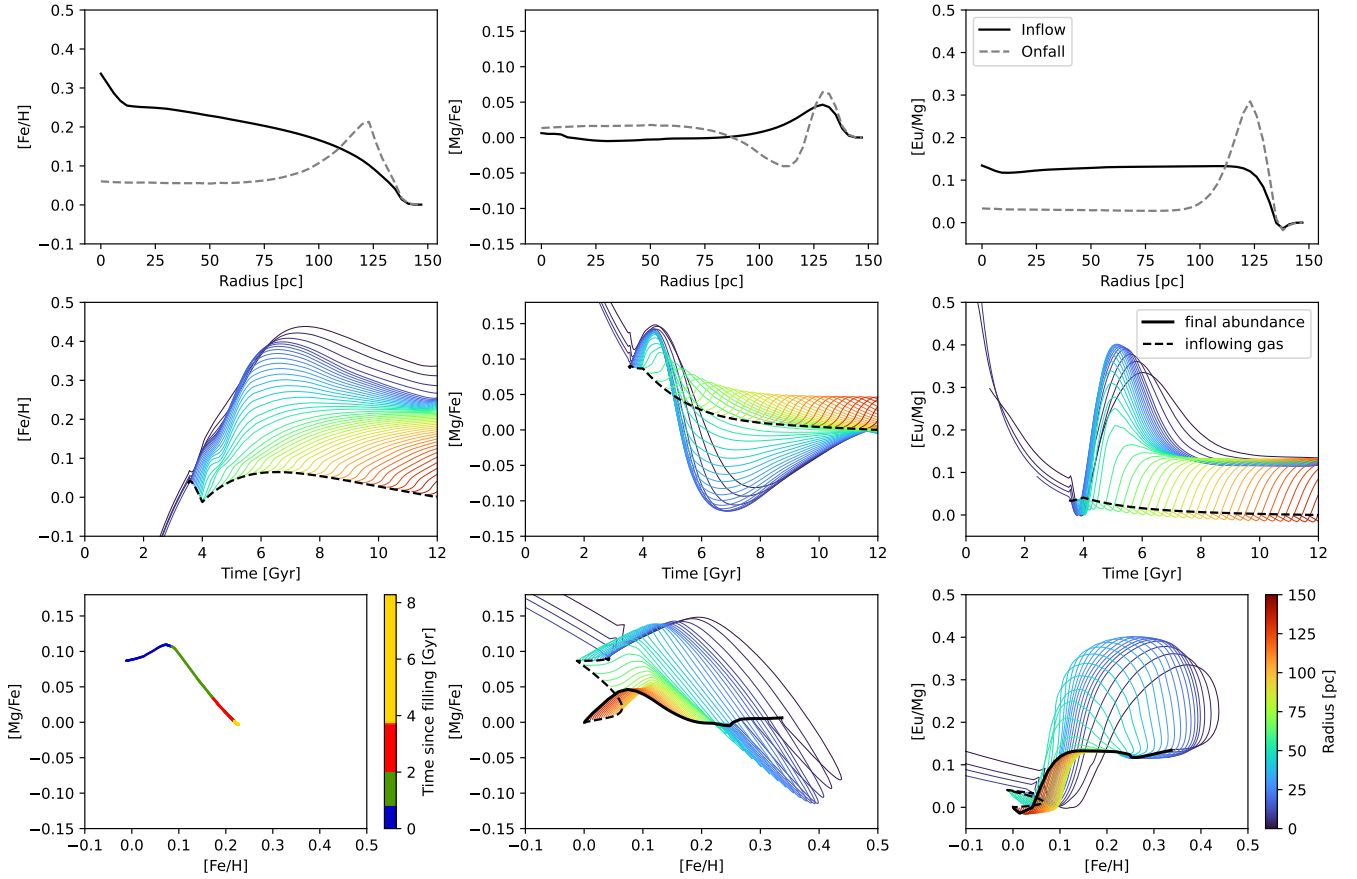


Figure 6. Same as Figure 5, but for the inflow instead of the onfall scenario. The bottom left plot shows ring 10.

funnelling gas from the bar tips. So at every timestep, each ring receives gas with the same abundance, which is lower in metals than the processed gas in the nuclear disc. By contrast, in the inflow model, fresh gas only reaches the nuclear ring and from there has to flow inwards through the nuclear disc.

Consequently, the inflow model shows a much larger accumulation of heavy elements, as the inflowing gas gets successively enriched on its way to the inside. Let us now look at the observable abundance patterns vs. radius at present time which we show in the top row of each figure. In both models there is an overall heavy element enhancement as well as a slight [Mg/Fe] and [Eu/Mg] overabundance which is owed to the hot gas phase losses in the nuclear disc that favours elements contributed by sources that inject more yields directly into the cold gas phase like ccSN or NSM (where $f_{c,NSM} > f_{c,ccSN}$).

The most prominent feature, especially in the onfall scenario, is the overabundance peak of the nuclear ring at the outer edge of the NSD. The rings around that radius have not yet completed their "loop" around the main trend due to the initial star burst, which leads to imprints in abundances that are slightly shifted due to the different onset times of the stellar death scenarios. (I.e. the outer side of the nuclear ring should be α -enriched, the inner one iron enriched and $[\alpha/Fe]$ poor.)

However, the main difference between the models is the flow bringing iron from the nuclear disc edge inwards in the inflow model. The onfall model shows a dip in [Mg/Fe] just inside the nuclear ring. This dip is filled by the high-[Mg/Fe] material flowing inwards from the ring in the inflow model. Similarly, the high [Eu/Mg] peak seen in the onfall model and created by the shifted onset of NSM and ccSN

distributes across the whole nuclear disc in the inflow model. Most directly, the difference is seen however in the large radial [Fe/H] gradient in the inflow model which stems from heavy elements being advected inwards with the flow.

4.4 Varying the parameters

After the discussion of main features in the last sections, we turn to varying the parameters guiding the global gas balances. Here, we mainly focus on the two ejection fractions, i.e. the fraction of yields that is lost to the CGM in the galactic and the nuclear disc.

4.4.1 Galactic disc ejection fraction

The ejection fraction to the CGM in a galaxy is a simplification for the observed mass loss of processed gas from starforming discs. We remind the reader also of the analytical solution for the equilibrium abundance of some element j , $Z_{j,eq}$, in an open box model:

$$Z_{j,eq} = Z_{j,y} \frac{(1 - e_s)r}{1 + \eta} \quad (4)$$

where $Z_{j,y}$ is the abundance of the stellar yields, e_s the ejection fraction of yields from the stars, η the outflow efficiency or ablation factor and r the recycling factor, i.e. the fraction of stellar yields that does not stay indefinitely locked up in low mass stars. In the real world, when the galactic disc loses a fraction of its yields, the lost gas mass is compensated by more metal-poor inflowing gas,

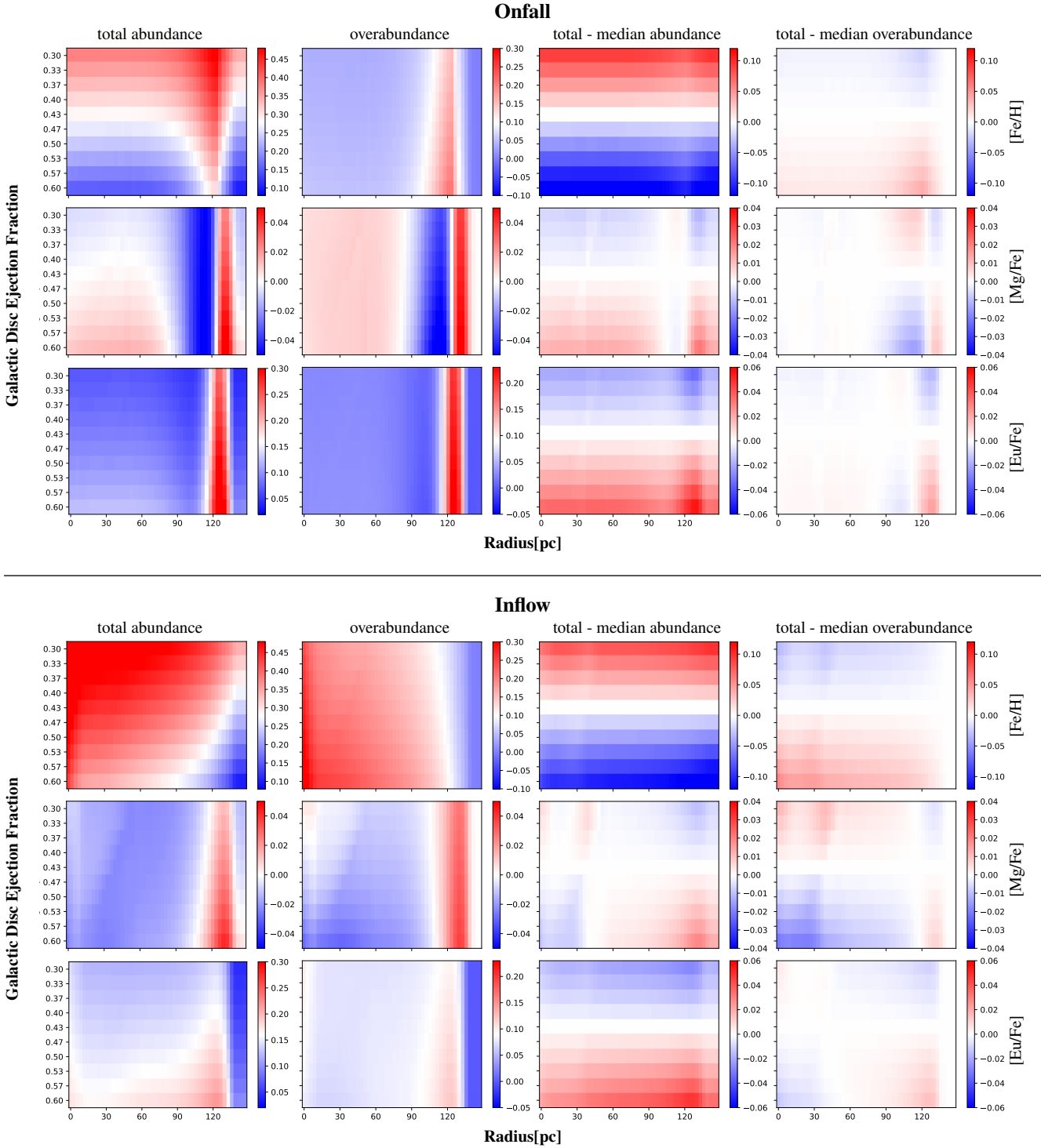


Figure 7. Effects of the galactic disc eject fraction on the $[\text{Fe}/\text{H}]$, $[\text{Mg}/\text{Fe}]$, $[\text{Eu}/\text{Fe}]$ abundance in the nuclear disc. Columns from the left: total abundance, overabundance over the final abundance at the tips of the Galactic bar at 4 kpc, and then total and total overabundance minus their median values.

lowering the metallicity similar to the ablation term η . Since the main galactic disc feeds the nuclear disc, lowering its metallicity also reduces elemental abundances in the nuclear disc.

We can trace this effect in [Figure 7](#), where we show the final values of $[\text{Fe}/\text{H}]$, $[\text{Mg}/\text{Fe}]$, and $[\text{Eu}/\text{Fe}]$ (note we here trace $[\text{Eu}/\text{Fe}]$ not $[\text{Eu}/\text{Mg}]$ as above) as a function of radius in the nuclear disc while varying the global loss rate between 30 and 60% (declining along the y-axis), with other parameters fixed (see [Table 2](#)). As before,

we compare the onfall and inflow models on top and bottom of the figure. In the plot we see in the left two columns the resulting abundance profiles (relative to solar and the tips of the bar respectively), whereas the right-hand side of the plot (columns 3 and 4) shows the (over)abundances relative to the standard parametrisation - hence a white line at loss fraction 0.43.

We first focus on the onfall model. The global loss rate strongly affects the overall metallicity, seen in $[\text{Fe}/\text{H}]$ (first row). However,

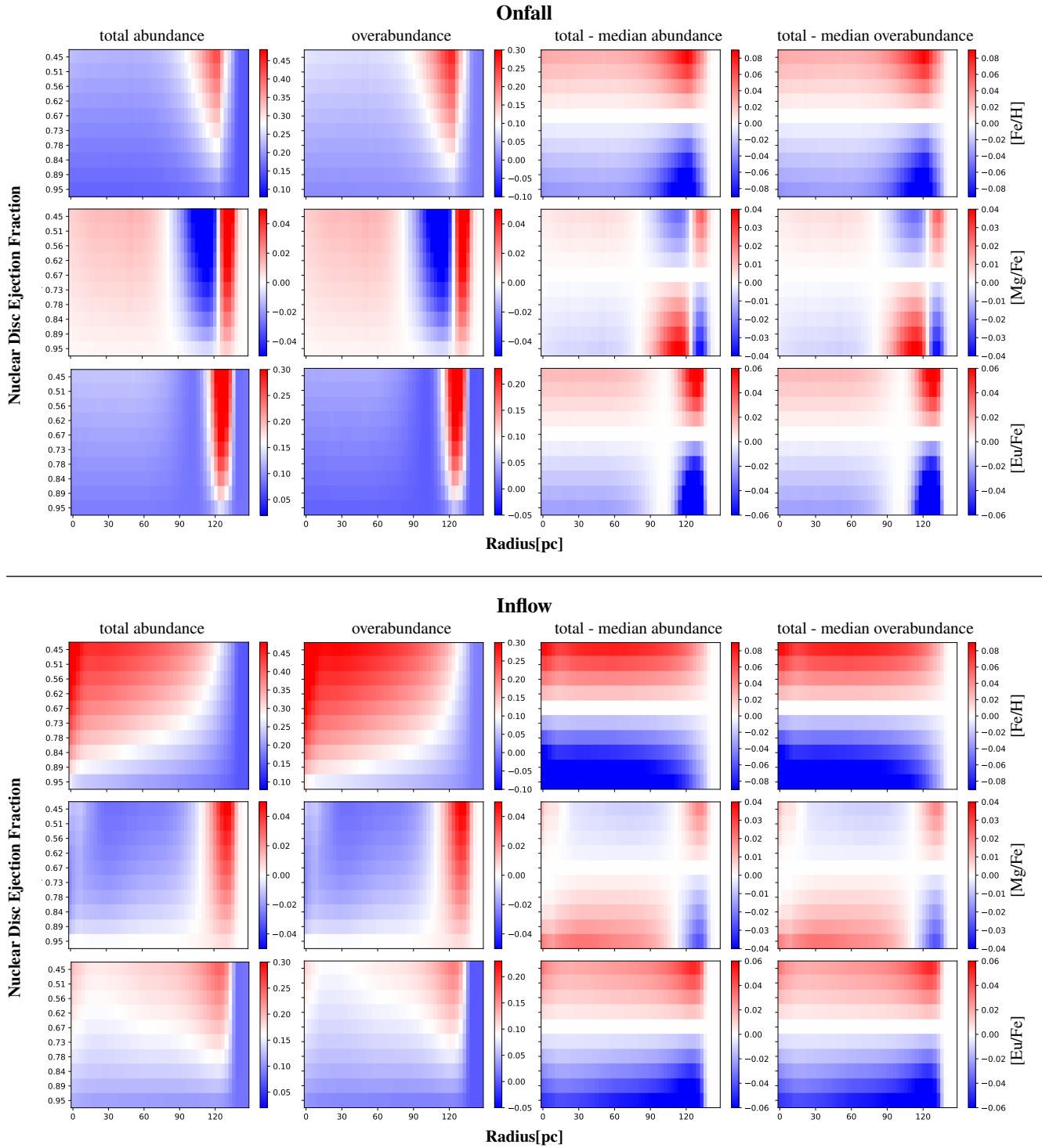


Figure 8. Effects of the nuclear eject fraction on the $[\text{Fe}/\text{H}]$, $[\text{Mg}/\text{Fe}]$, $[\text{Eu}/\text{Fe}]$ abundance in the nuclear disc. The columns are the same as in [Figure 7](#)

also the abundance ratios $[\text{Mg}/\text{Fe}]$ and $[\text{Eu}/\text{Fe}]$ show a weak effect. However, due to different hot gas fractions between ccSN/NSM and SNIa, iron is most strongly affected as its retention in the NSD is most strongly suppressed. This seems at first concerning, since the global loss rate is not well-constrained in chemical evolution. However, this is greatly helped by using the relative overabundances relative to the bar tips (2nd/4th column in [Fig. 7](#)), which reduces the effect by about 1 order of magnitude. In the onfall scenario, the remaining change is quite straight-forward (focus on the 4th column, which focuses on

the changes between models by subtracting the median abundance profile): increasing the global loss rate lowers the overall baseline abundance, so $[\text{Fe}/\text{H}]$ overabundances in the nuclear disc come out slightly more strongly. On the abundance ratios, the same effect exacerbates slightly the overabundance pattern at smaller loss rates: We see a pronounced lowering of the $[\text{Mg}/\text{Fe}]$ ratio and a (due to the smaller difference in timescales between NSM and SNIa than ccSN and SNIa) milder lowering of $[\text{Eu}/\text{Fe}]$ directly within the nuclear ring, where the star formation rate is dropping steeply as the ring

expands outwards. This means higher current Fe production, and so a lower baseline metallicity lowers [Mg/Fe] ratios behind the ring. At the same time, the relative overabundance on the star forming nuclear ring is stronger at higher loss rates, again because in this case, the current star formation burst on the ring has a stronger effect on the gas abundances.

Subtracting the median profile (in column 4 of Figure 7) allows us to track the changes in overabundance undistracted by the specific abundance pattern in each case and shows that the changes in overabundance are a simple consequence of the outer disc abundance change. We see again that in the inflow scenario effects (e.g. here from the galactic disc ejection fraction) build up towards the inside and are overall retained longer, while they are drowned out by onfalling gas in the onflow case. As expected from such a baseline effect, the changes in overabundance are almost an order of magnitude smaller than the changes in absolute abundance which stresses another time that the abundance difference to the bar tips is key to understanding nuclear disc chemistry.

4.4.2 Nuclear disc loss rates

For comparison, we now look at the effect of the nuclear disc ejection fraction (see Figure 8). The general effect is easy to understand: If less of the yields from dying stars are retained, the corresponding ISM abundances decrease. This is true for all our considered elements. As this parameter only affects the nuclear disc, taking the overabundance does not wash it out and its consequences are fully seen in the overabundances vs. the bar tips (2nd and 4th column).

The right-most column of Figure 8 shows that to first order lower nuclear disc ejection fractions just result in correspondingly larger overabundances. To second order, in the inflow model, a larger nuclear disc ejection fraction reduces the present gas mass as the inflow speed is limited in our model. However, from the figure we judge this effect on the abundances as rather minor.

5 CONCLUSION

We have presented the first spatially resolved chemodynamical model of the nuclear stellar disc, embedded in a full galactic chemical evolution model. The model incorporates an exponential nuclear gas disc, a nuclear ring with intense star formation on the edge of the nuclear disc and a flow of gas funnelled down from the tips of the bar region, sustaining the intense star formation in the nuclear disc.

Such chemical evolution models help constrain the star formation history and genesis of a system. More importantly, chemical evolution models translate the flows of gas, i.e. the accretion of gas, the loss of stellar yields from a component, and the internal flows of gas (i.e. radial redistribution) into observable time- and radius-dependent abundance patterns, the simplest of which is the present-day abundance profiles of the cold star-forming gas.

As a first study, we have examined the main features expected for the abundance profiles in the nuclear disc in different scenarios for the gas flow. We have dissected the enrichment history and found that the nuclear disc chemical history is dominated by the lasting effect of the strongly star forming, outwards moving nuclear ring. We have also shown that one should study the abundances of the nuclear disc relative to the bar tips from where the gas is funnelled.

Our models show a mild enrichment of overall heavy element abundances relative to the tips of the bar from which gas is flowing down, and an enrichment particularly in [Mg/Fe] and [Eu/Fe] at the

dense star-forming nuclear ring.⁴ This peak is caused by the sudden rise of star formation efficiency experienced by the infalling gas and the outward expansion of the star-forming ring. As α -element enrichment is near-instantaneous, and iron enrichment from SNIa lags by ~ 1 Gyr, this ring structure is followed by a dip in [Mg/Fe] at slightly smaller radius (where the star-formation rate is dropping). Eu (an r-process element from neutron star mergers) has an intermediate production timescale and so the peak-dip structure is slightly shifted to smaller radii, with the possibility of additionally lowered [Eu/Fe] ratios on the outer edge of the ring, where ccSN contribute iron, before the NSM driven r-process yields kick in.

Our main focus is showing how two principal flow patterns in the nuclear disc affect the results: an onfall-scenario, where the gas is funnelled from the bar onto all parts of the nuclear disc directly, and an inflow scenario, where the funnelled gas is deposited on the nuclear ring and then flows inwards through the nuclear disc. The inflow scenario shows marked differences. In particular, the radially inward flow of gas in the inflow model distributes the radial structures of abundance ratios further inwards and leads to a pile-up of heavy elements towards the inner nuclear disc. This results in a significant gradient of nuclear disc metallicity, which is much weaker or absent in the onfall model.

We have also shown that the overall enrichment history of the galactic disc affects the nuclear disc, which just reprocesses the funnelled-in gas. Depending on nuclear disc formation time, the initial rise in galactic metallicity and decline in [Mg/Fe] ([Eu/Mg]) ratios translates into lower nuclear disc metallicity and higher [Mg/Fe] ([Eu/Mg]) if it forms earlier. This shift directly translates to the measurements against the current bar tips.

At later times the bar tips expanding further into the negative radial metallicity gradient will imply a slow decrease in metallicity of the funnelled gas, which is mirrored in the nuclear stellar disc by a significant negative stellar radial metallicity gradient.

Ultimately, understanding the nuclear disc will involve major studies of parameter variations in models like ours. As an example we have here studied how the galactic disc yield ejection fraction and the yield ejection fraction in the nuclear disc affect its present-day abundances. This study particularly underlined the value of studying abundances of the nuclear disc relative to the bar tips, which largely eliminate the impact of nuisance outer disc chemical evolution parameters like its ejection rate and helps study the chemical evolution of the nuclear disc with better focus. We also note that such a relative abundance study will reduce the large systematic biases in abundance measurements.

In the future, models, like the presented, will serve to constrain galactic gas flows and structure. To just name two examples: we currently know little about the gas flows into the galactic centre and their long-term angular momentum balance, as only a fraction of the funnelled gas actually ends up in stars (and much less in the central black hole). A major part will be expelled in winds and we have shown that this kind of gas loss can be directly quantified by abundance differences. Secondly, the nuclear disc is a unique laboratory with very little space for retaining hot gas close to the nuclear disc, which implies that most of its hot gas should be expelled in the galactic fountain. This in turn means that comparing nuclear

⁴ One caveat is needed here: If there is more gas from the bar/bulge, or if somehow significant amounts of gas can be accreted onto the nuclear disc (a scenario we currently see no reason to adopt), this would result in overall lower metallicity (currently only the outermost fringe in our model nuclear disc is slightly lower than the bar), but we do not expect major changes in the abundance ratios.

stellar disc data with our models, we expect to be able to break the degeneracies in assessing what stellar types contribute in which fraction to the cold/hot gas phases, central to understanding early galactic enrichment. We will treat this in depth in a future paper.

Now, there is plenty of caveats that should be named in such a work. Of course, the usual caveats of chemical evolution models, e.g. assumptions of stellar yields, IMF assumptions, etc. should be regularly revisited. Those are important, but we expect them to have lesser impact on the statements we make in this paper. The more unsettling parts are the uncertainties in both theory and observations: On the theoretical side, little modelling has been done for nuclear discs, especially of the stellar contribution. In particular, it is unclear how stars in the nuclear disc get re-distributed e.g. in radius: there is some spiral structures observed, but there is currently no measure for radial migration, heating, and related processes. Due to this uncertainty we here showed mainly abundance profiles for the star-forming gas for which stellar migration plays a subordinate role compared to gas flows (as shown in many galactic disc papers).

Additionally, it remains unknown how much gas from the bar area (e.g. stellar yields, coronal accretion) is swept up during the funnelling and pollutes the inflowing gas. Further, we make our predictions depending on parameters currently in a rather observation-free space, as we lack resolved, high-quality observations for both stellar abundance patterns and also present-day star-forming gas abundances in the nuclear disc. So, this paper should also be taken as a strong encouragement to push for better data: nuclear discs can help in constraining important galactic processes, but this is only possible, once we can challenge models like ours with high-quality data.

ACKNOWLEDGEMENTS

We thank Jack Fraser-Govil and Mike Rich for helpful discussions. JF acknowledges support from University College London's Graduate Research Scholarship. RS thanks the Royal Society for generous support via a University Research Fellowship.

DATA AVAILABILITY

The code underlying this article is available on GitHub under https://github.com/JFriske/RAMICES_II, we will be happy to provide any data underlying the figures and more upon request to the corresponding author.

REFERENCES

Abdurro'uf et al., 2022, *ApJS*, 259, 35
 Alpher R. A., Bethe H., Gamow G., 1948, *Phys. Rev.*, 73, 803
 Arnett W. D., Clayton D. D., 1970, *Nature*, 227, 780
 Athanassoula E., 1992, *MNRAS*, 259, 345
 Athanassoula E., Misiriotis A., 2002, *MNRAS*, 330, 35
 Aumer M., Schönrich R., 2015, *MNRAS*, 454, 3166
 Baba J., Kawata D., 2020, *MNRAS*, 492, 4500
 Bacon R., et al., 2001, *MNRAS*, 326, 23
 Bally J., Stark A. A., Wilson R. W., Henkel C., 1988, *ApJ*, 324, 223
 Bania T. M., 1977, *ApJ*, 216, 381
 Berentzen I., Shlosman I., Martínez-Valpuesta I., Heller C. H., 2007, *ApJ*, 666, 189
 Bilitewski T., Schönrich R., 2012, *MNRAS*, 426, 2266
 Binney J., Tremaine S., 2008, *Galactic Dynamics: Second Edition*
 Binney J., Gerhard O., Spergel D., 1997, *MNRAS*, 288, 365
 Bittner A., et al., 2020, *A&A*, 643, A65

Bland-Hawthorn J., Cohen M., 2003, *ApJ*, 582, 246
 Burbidge E. M., Burbidge G. R., Fowler W. A., Hoyle F., 1957, *Rev. Mod. Phys.*, 29, 547
 Buta R., Combes F., 1996, *Fundamentals of Cosmic Physics*, 17, 95
 Cescutti G., 2008, *A&A*, 481, 691
 Chabrier G., 2003, *Publications of the Astronomical Society of the Pacific*, 115, 763
 Chandrasekhar S., Milne E. A., 1931, *MNRAS*, 91, 456
 Chatzopoulos S., Fritz T. K., Gerhard O., Gillessen S., Wegg C., Genzel R., Pfuhl O., 2015, *MNRAS*, 447, 948
 Chiba R., Schönrich R., 2021, *MNRAS*, 505, 2412
 Chiba R., Friske J. K. S., Schönrich R., 2020, *MNRAS*, 500, 4710
 Chornock R., et al., 2017, *ApJL*, 848, L19
 Clayton D. D., Fowler W. A., Hull T. E., Zimmerman B. A., 1961, *Annals of Physics*, 12, 331
 Colavitti E., Matteucci F., Murante G., 2008, *A&A*, 483, 401
 Combes F., Gerin M., 1985, *A&A*, 150, 327
 Comerón S., Knapen J. H., Beckman J. E., Laurikainen E., Salo H., Martínez-Valpuesta I., Buta R. J., 2010, *MNRAS*, 402, 2462
 Contopoulos G., Grosbøl P., 1989, *A&A Rev.*, 1, 261
 Crowther P. A., 2007, *ARA&A*, 45, 177
 Côté B., et al., 2018, *ApJ*, 855, 99
 Côté B., et al., 2019, *ApJ*, 875, 106
 Debattista V. P., Sellwood J. A., 2000, *ApJ*, 543, 704
 Dobler G., Finkbeiner D. P., Cholis I., Slatyer T., Weiner N., 2010, *ApJ*, 717, 825
 Dubinski J., Berentzen I., Shlosman I., 2009, *ApJ*, 697, 293
 Emsellem E., et al., 2022, *A&A*, 659, A191
 Englmaier P., Gerhard O., 1999, *MNRAS*, 304, 512
 Erwin P., 2004, *A&A*, 415, 941
 Feldmeier-Krause A., Kerzendorf W., Neumayer N., Schödel R., Nogueras-Lara F., Do T., de Zeeuw P. T., Kuntschner H., 2017, *MNRAS*, 464, 194
 Ferrière K. M., 2001, *Reviews of Modern Physics*, 73, 1031
 Fink M., Röpké F. K., Hillebrandt W., Seitzzahl I. R., Sim S. A., Kromer M., 2010, *A&A*, 514, A53
 Fragkoudi F., et al., 2019, *MNRAS*, 488, 3324
 Fraser J., Schönrich R., 2021, *MNRAS*, 509, 6008
 Frischknecht U., Hirschi R., Thielemann F. K., 2012, *A&A*, 538, L2
 Friske J., Schönrich R., 2019, *MNRAS*, 490, 5414
 Fritz T. K., et al., 2021, *A&A*, 649, A83
 Fux R., 1999, *A&A*, 345, 787
 Gadotti D. A., et al., 2020, *A&A*, 643, A14
 Goetz M., Koeppen J., 1992, *A&A*, 262, 455
 Grieco V., Matteucci F., Ryde N., Schultheis M., Uttenthaler S., 2015, *MNRAS*, 450, 2094
 Groves B., et al., 2023, *MNRAS*, 520, 4902
 Hotokezaka K., Beniamini P., Piran T., 2018, *International Journal of Modern Physics D*, 27, 1842005
 Hoyle F., 1954, *APJS*, 1, 121
 Iben I., Tutukov A. V., 1984, *APJS*, 54, 335
 Iben I., Tutukov A. V., 1987, *ApJ*, 313, 727
 Iwamoto K., Brachwitz F., Nomoto K., Kishimoto N., Umeda H., Hix W. R., Thielemann F.-K., 1999, *ApJS*, 125, 439
 Jiang J.-a., et al., 2017, *Nature*, 550, 80
 Johnson H. M., 1957, *ApJ*, 62, 19
 Kalberla P. M. W., Dedes L., 2008, *A&A*, 487, 951
 Karlsson T., 2005, *A&A*, 439, 93
 Kennicutt Jr. R. C., 1998, *ApJ*, 498, 541
 Kennicutt R. C., Lee J. C., Akiyama S., Funes J. G., Sakai S., 2005, in Hüttmeister S., Manthey E., Bomans D., Weis K., eds, *American Institute of Physics Conference Series Vol. 783, The Evolution of Starbursts*. pp 3–16, doi:10.1063/1.2034960
 Knapen J. H., Laine S., Relaño M., 1999, *Astrophysics and Space Science*, 269, 605
 Krause M. G. H., Rodgers-Lee D., Dale J. E., Diehl R., Kobayashi C., 2021, *MNRAS*, 501, 210

Kromer M., Sim S. A., Fink M., Röpké F. K., Seitzzahl I. R., Hillebrandt W., 2010, *ApJ*, 719, 1067
 Lacey C. G., Fall S. M., 1985, *ApJ*, 290, 154
 Launhardt R., Zylka R., Mezger P. G., 2002, *A&A*, 384, 112
 Liszt H. S., Burton W. B., 1978, *ApJ*, 226, 790
 Livio M., Mazzali P., 2018, *Physics Reports*, 736, 1
 Longmore S. N., et al., 2013, *MNRAS*, 429, 987
 Maciejewski W., Teuben P. J., Sparke L. S., Stone J. M., 2002, *MNRAS*, 329, 502
 Magg E., et al., 2022, *A&A*, 661, A140
 Majewski S. R., et al., 2017, *AJ*, 154, 94
 Martínez-Valpuesta I., Shlosman I., Heller C., 2006, *ApJ*, 637, 214
 Matteucci F., Chiosi C., 1983, *A&A*, 123, 121
 Mayer L., Kazantzidis S., Escala A., 2008, *Memorie della Società Astronomica Italiana*, 79, 1284
 McWilliam A., Zoccali M., 2010, *ApJ*, 724, 1491
 Moon S., Kim W.-T., Kim C.-G., Ostriker E. C., 2023, *ApJ*, 946, 114
 Nataf D. M., Udalski A., Gould A., Fouqué P., Stanek K. Z., 2010, *ApJL*, 721, 28
 Nesvada N. P. H., Boulanger F., Lehnert M. D., Guillard P., Salome P., 2011, *A&A*, 536, L5
 Nogueras-Lara F., 2022, *A&A*, 668, L8
 Nogueras-Lara F., et al., 2023a, *arXiv230907219N*
 Nogueras-Lara F., Schultheis M., Najarro F., Sormani M. C., Gadotti D. A., Rich R. M., 2023b, *A&A*, 671, L10
 Nomoto K., Thielemann F. K., Yokoi K., 1984, *ApJ*, 286, 644
 Nomoto K., Kobayashi C., Tominaga N., 2013, *ARA&A*, 51, 457
 Pagel B. E. J., Patchett B. E., 1975, *MNRAS*, 172, 13
 Petters III W. L., 1975, *ApJ*, 195, 617
 Pignatari M., Gallino R., Meynet G., Hirschi R., Herwig F., Wiescher M., 2008, *ApJ*, 687, L95
 Portinari L., Chiosi C., 2000, *A&A*, 355, 929
 Rauscher T., Patkos A., 2010, *Handbook of Nuclear Chemistry*, pp 611–665
 Rougoor G. W., Oort J. H., 1960, *Proceedings of the National Academy of Sciences*, 46, 1
 Schmidt M., 1959, *ApJ*, 129, 243
 Schultheis M., et al., 2021, *A&A*, 650, A191
 Schönrich R., Binney J., 2009, *MNRAS*, 396, 203
 Schönrich R., McMillan P. J., 2017, *MNRAS*, p. stx093
 Schönrich R., Weinberg D. H., 2019, *MNRAS*, 487, 580
 Schönrich R., Aumer M., Sale S. E., 2015, *ApJL*, 812, L21
 Seidel M. K., Falcón-Barroso J., Martínez-Valpuesta I., Sánchez-Blázquez P., Pérez I., Peletier R., Vazdekis A., 2016, *MNRAS*, 460, 3784
 Sellwood J. A., Gerhard O., 2020, *MNRAS*, 495, 3175
 Sharples R., et al., 2013, *The Messenger*, 151, 21
 Simkin S. M., Su H. J., Schwarz M. P., 1980, *ApJ*, 237, 404
 Soker N., 2018, *Science China: Physics, Mechanics and Astronomy*, 61, 9144
 Sorlin O., Porquet M. G., 2008, *Progress in Particle and Nuclear Physics*, 61, 602
 Sormani M. C., Sobacchi E., Fragkoudi F., Ridley M., Treß R. G., Glover S. C. O., Klessen R. S., 2018, *MNRAS*, 481, 2
 Sormani M. C., et al., 2022, *MNRAS*, 512, 1857
 Sormani M. C., et al., 2023, *MNRAS*, 523, 2918
 Spagna A., Lattanzi M. G., Fiorentin P. R., Smart R. L., 2010, *A&A*, 510, L4
 Stanek K. Z., Mateo M., Udalski A., Szymanski M., Kaluzny J., Kubiak M., 1994, *ApJ*, 429, L73
 Su M., Slatyer T. R., Finkbeiner D. P., 2010, *ApJ*, 724, 1044
 Sánchez-Blázquez P., et al., 2014, *A&A*, 570, A6
 Thielemann F., Nomoto K., Yokoi K., Thielemann F. K., Nomoto K., Yokoi K., 1986, *A&A*, 158, 17
 Thorsbro B., et al., 2020, *ApJ*, 894, 26
 Tinsley B. M., 1979, *ApJ*, 229, 1046
 Wang B., Han Z., 2012, *New Astronomy Reviews*, 56, 122
 Whelan J., Iben Jr. I., 1973, *ApJ*, 186, 1007
 Wylie S. M., Clarke J. P., Gerhard O. E., 2022, *A&A*, 659, A80
 Yang H. Y., Ruzsowski M., Zweibel E. G., 2018, *Galaxies*, 6, 29
 van de Ven G., Chang P., 2009, *ApJ*, 697, 619

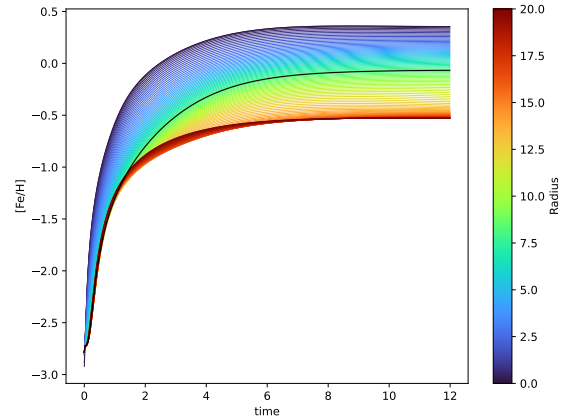


Figure A1. Global Iron Abundance. The abundance of the solar annulus is highlighted in black.

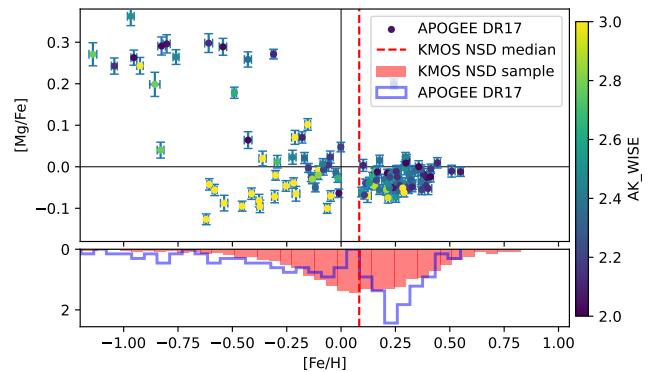


Figure A2. Comparison of the APOGEE DR17 (Abdurro'uf et al. 2022) stars with WISE reddening $AK_WISE > 2$ and passing recommended quality checks, and the KMOS NSD sample from Schultheis et al. (2021).

APPENDIX A: SOME EXTRA MATERIAL

This Appendix serves to deliver material that the reader might wonder about, but which was not directly pertaining to our main discussion.

Fig. A1 shows the abundance of $[Fe/H]$ vs. time for the main galactic disc at different radii (colour code). Two main qualities are important for the discussion in this paper: $[Fe/H]$ shows an initial rise towards a plateau covering the last ~ 8 Gyrs of evolution. The initial rise may be inherited by the NSD if the bar formation time falls into that period. Further, the galaxy has a strong radial abundance gradient of order -0.06 dex kpc^{-1} in concordance with Cepheid data. As the bar grows, the bar tips move outwards and the covered radial abundance gradient will be reflected by a corresponding negative nuclear disc abundance gradient if the nuclear disc grows inside-out (as set in our models).

Fig. A2 shows the problematic situation with current Milky Way NSD data from Apogee vs. KMOS (Abdurro'uf et al. 2022; Fritz et al. 2021). It is instantly apparent that the selected APOGEE stars' metallicity distribution does not match the KMOS derived metallicity distribution. Moreover, the abundances of the APOGEE disc stars in $[Mg/Fe]$ seem to show a negative correlation between extinc-

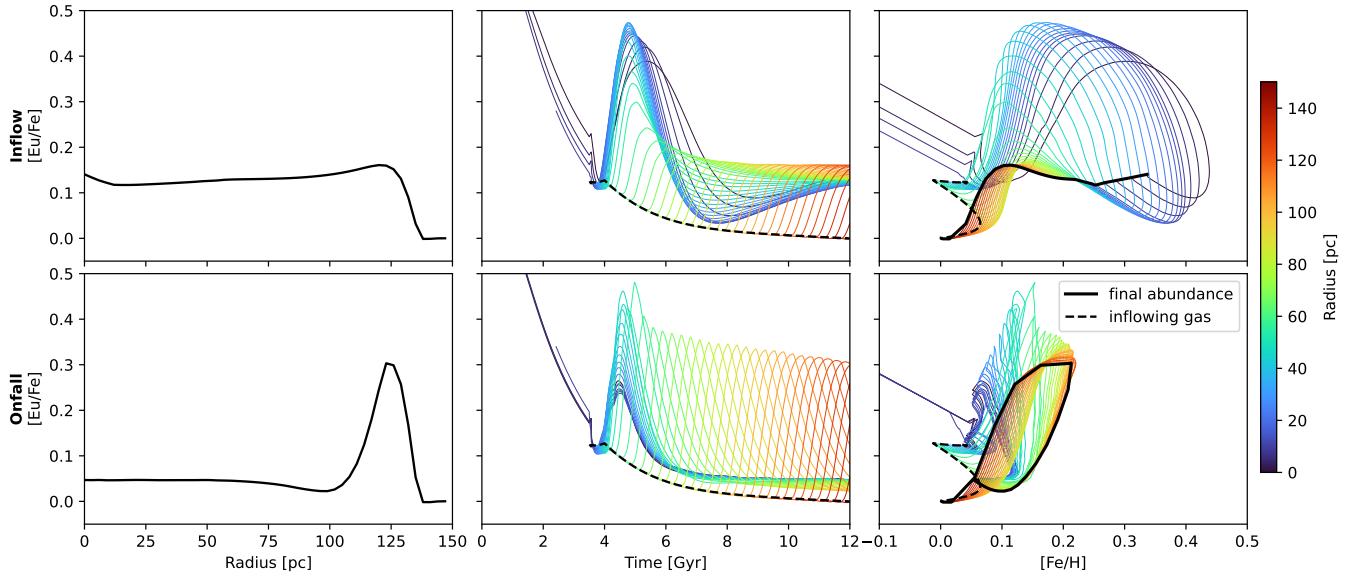


Figure A3. Comparison of the inflow and onfall scenario in $[\text{Eu}/\text{Fe}]$

tion and metallicity. By plotting for the whole survey abundances vs. extinction and effective stellar temperature, we could ascertain that stars at high reddening and low temperature, i.e. basically all stars in the NSD in APOGEE, show concerning abundance and metallicity trends. Stars with high metallicity, low temperature and high extinction are particularly difficult to analyse, so we conclude that at least the shown Apogee abundances require thorough revision and can currently not be used for a model comparison.

Fig. A3 adds to the NSD detailed abundance models shown in Figure 5 and Figure 6 by showing in addition the $[\text{Eu}/\text{Fe}]$ ratios (instead of $[\text{Eu}/\text{Mg}]$) for both the Onfall (top row) and Inflow (bottom row) models.

This paper has been typeset from a \LaTeX file prepared by the author.